

Detection of planet candidates around K giants [★] HD 40956, HD 111591, and HD 113996

G. Jeong^{1,2}, B.-C. Lee^{1,2} ^{★★}, I. Han^{1,2}, M. Omiya³, H. Izumiura^{3,4}, B. Sato⁵, H. Harakawa³, E. Kambe⁴ and D. Mkrtichian⁶

¹ Korea Astronomy and Space Science Institute, 776, Daedeokdae-Ro, Youseong-Gu, Daejeon 34055, Korea
e-mail: [tlotv;bcllee;iwhan]@kasi.re.kr

² Korea University of Science and Technology, 217, Gajeong-ro, Yuseong-gu, Daejeon 34113, Korea

³ National Astronomical Observatory of Japan, 2-21-1 Osawa, Mitaka, Tokyo 181-8588, Japan
e-mail: [omiya.masashi;h.harakawa]@nao.ac.jp

⁴ Okayama Astrophysical Observatory, National Astronomical Observatory of Japan, 3037-5 Honjo, Kamogata, Asakuchi, Okayama 719-0232, Japan
e-mail: [izumiura;kambe]@oao.nao.ac.jp

⁵ Department of Earth and Planetary Sciences, Tokyo Institute of Technology, 2-12-1 Okayama, Meguro-ku, Tokyo 152-8551, Japan
e-mail: satobn@geo.titech.ac.jp

⁶ National Astronomical Research Institute of Thailand, Siriphanich Bldg., Chiang Mai, Thailand
e-mail: davidmkr@gmail.com

Received 28 June 2016 / Accepted 18 October 2017

ABSTRACT

Aims. The purpose of this paper is to detect and investigate the nature of long-term radial velocity (RV) variations of K-type giants and to confirm planetary companions around the stars.

Methods. We have conducted two planet search programs by precise RV measurement using the 1.8 m telescope at Bohyunsan Optical Astronomy Observatory (BOAO) and the 1.88 m telescope at Okayama Astrophysical Observatory (OAO). The BOAO program searches for planets around 55 early K giants. The OAO program is looking for 190 G–K type giants.

Results. In this paper, we report the detection of long-period RV variations of three K giant stars, HD 40956, HD111591, and HD113996. We investigated the cause of the observed RV variations and conclude the substellar companions are most likely the cause of the RV variations. The orbital analyses yield $P = 578.6 \pm 3.3$ d, $m \sin i = 2.7 \pm 0.6 M_J$, $a = 1.4 \pm 0.1$ AU for HD 40956; $P = 1056.4 \pm 14.3$ d, $m \sin i = 4.4 \pm 0.4 M_J$, $a = 2.5 \pm 0.1$ AU for HD 111591; $P = 610.2 \pm 3.8$ d, $m \sin i = 6.3 \pm 1.0 M_J$, $a = 1.6 \pm 0.1$ AU for HD113996.

Key words. stars: individual: HD 40956, HD 111591, HD 113996 — stars: planetary systems — techniques: radial velocities

1. Introduction

Planetary formation around normal stars involves complex processes that depend on various stellar properties: stellar mass, metallicity, radiation flow of central stars, the host star's environment, binarity, and so on. An understanding of the planetary formation can be done only if the effects of these stellar parameters are disentangled. To do this it is necessary to search for planets around stars with a wide range of stellar properties (especially stellar mass). However, the majority of exoplanets have been detected around solar-type main sequence stars by radial velocity (RV) and transit methods.

Fifteen years ago, we had only limited knowledge about exoplanets around intermediate-mass stars with stellar masses of more than $1.5 M_\odot$. The intermediate-mass main sequence stars are not suitable targets for precise RV measurements because they have few absorption lines that are often broadened due to high stellar-rotation rates. Although some precise Doppler surveys searching for planets around intermediate-mass stars had been conducted, we didn't know how each process in the plan-

etary formation depends on the stellar mass larger than $1.5 M_\odot$. However, recently, the Doppler surveys of G- and K-type giant stars located in the red clump on the H-R diagram have uncovered the properties of planetary systems around intermediate-mass stars because the giants are evolved intermediate-mass stars with slower rotations and lower temperatures suitable for precise RV measurements (e.g., [Sato et al. 2012](#)).

Beginning with the first hints of possible planets around K giant stars (β Gem) found by [Hatzes & Cochran \(1993\)](#), the discovery of the giant planet around ι Dra by [Frink et al. \(2002\)](#) is largely considered as the first confirmed planet around a giant star. The number of planets orbiting giant stars is increasing and more than 95 planets have been detected so far. Stellar properties of the planet-hosting giants have been understood with a significantly large sample. Based on a Doppler survey of 373 G- and K-type giants, [Reffert et al. \(2015\)](#) found that the planet occurrence rate of intermediate-mass stars depends on stellar masses, and the rate reaches its maximum at a stellar mass of $1.9 M_\odot$ and drops off at stellar masses of more than $2.7 M_\odot$. They concluded that no giant planet has been found around stars more massive than $2.7 M_\odot$ and suggested that the giant planet formation and/or inward migration in protoplanetary disks are sup-

[★] Based on observations made with the BOES at BOAO in Korea and HIDES at OAO in Japan.

^{★★} Corresponding author : B. -C. Lee

pressed for more massive stars because of fast disk depletion and/or the long migration time scale of giant planets.

The photometric transit method may be more favorable for Jupiter-type exoplanet detection around rapidly rotating early-type stars. However, only five planets have been found around F- and A-type stars; WASP-33 (Collier Cameron et al. 2010), KOI 13 (Ford et al. 2011), HAT-P-57 (Hartman et al. 2015), HAT-P-67 (Zhou et al. 2017), KELT-17 (Zhou et al. 2016) and KELT-9b (Gaudi et al. 2017), and some of them have been confirmed by the spectroscopic transiting method using Doppler Tomography. Thus, the most significant planet searches for giant planets around intermediate-mass stars are precise Doppler surveys of evolved giant stars.

Since 2003, we have been carrying out a precise RV survey of 55 K0–K4-type giants to investigate RV variations of K giant stars and to search for planets around the stars (Han et al. 2008, 2010) using the 1.8 m telescope at Bohyunsan Optical Astronomy Observatory (BOAO) and the Bohyunsan Observatory Echelle Spectrograph (BOES). To date we have discovered nine planet candidates around K giant stars (e.g., Lee et al. 2014a).

The East-Asian Planet Search Network, EAPS-Net (Izumiura 2005) is an international collaboration to search for planets around intermediate-mass G- and K-type (sub)giants using the 2 m-class telescopes in China, Japan, and Korea. In the framework of the EAPS-Net, the Korean-Japanese planet search program has been performed using the 1.8 m telescope at BOAO and BOES in Korea and the 1.88 m telescope at Okayama Astrophysical Observatory (OAO) and the High Dispersion Echelle Spectrograph (HIDES) in Japan (Omiya et al. 2009, 2012). In the program, 80 and 110 giants have been monitored at BOAO and OAO, respectively. We have also made intensive follow-up observations for candidate stars at both observatories to determine orbital parameters.

This paper is organized as follows. In Section 2, we describe the RV observations using the BOAO and OAO telescopes. Stellar properties and orbital solution of the planets are presented in Sections 3 and 4. In Section 5, we investigate the cause of radial velocity variations by *HIPPARCOS* photometry, chromospheric activity, and line shape analysis. Section 6 contains the summary and conclusion of this paper.

2. RV Observations

2.1. BOES observations

At BOAO, we have performed spectroscopic observations using the 1.8 m telescope and the Bohyunsan Observatory Echelle Spectrograph (BOES; Kim et al. 2007), which is a fiber-fed high-resolution echelle spectrograph. Using the BOES, we collected 22, 24, and 64 data points for HD 40956, HD 111591, and HD 113996, respectively. The data of HD 40956 and HD 111591 were obtained with the 200 μm fiber, giving a spectral resolution of 45,000. The typical exposure time of the observations is around 20 minutes, which can achieve a signal to noise ratio (S/N) of more than 150. HD 113996 was observed by the 80 μm fiber, giving a spectral resolution of 90,000. The average exposure time was 8 minutes to get a S/N of about 150.

One-dimensional (1D) spectra were extracted from the two-dimensional (2D) raw frames using standard Image Reduction and Analysis Facility (IRAF) procedures for bias subtraction, flat fielding, scattered light correction, spectrum extraction, and ThAr wavelength calibration. Precise RV measurements were performed by the program RVI2CELL (Han et al. 2007). The

long-term RV accuracy of BOES is about 7 m s^{-1} which is estimated by long-term monitoring of a RV standard star τ Ceti (Lee et al. 2013). We also use a pure high-resolution spectrum taken without the I_2 cell by BOES to determine stellar parameters.

2.2. HIDES observations

We also made RV observations of HD 40956 and HD 111591 in the framework of the Korean-Japanese planet search program using the 1.88 m telescope and the High Dispersion Echelle Spectrograph (HIDES, Izumiura 1999, Kambe et al. 2013) at OAO. In December 2007, HIDES CCD system was upgraded from a single 2k x 4k CCD to a mosaic CCD system (three 2k x 4k CCDs) covering a wide wavelength range of 3800–7500 \AA , which is three times larger than before. Although we made the observations using a slit mode of the HIDES until 2011 (HIDES-slit), HIDES was also upgraded to add a fiber-fed mode using a fiber-fed system attached to the Cassegrain focus of the telescope (HIDES-fiber). For precise RV measurements of our targets, we used an I_2 cell put in front of the slit and the fiber entrance for HIDES-slit and HIDES-fiber modes, respectively (Kambe et al. 2002). We set a slit width at 0.76 arcsec, giving a spectral resolution of 63,000 when we used the HIDES-slit mode. Using the 100 μm fiber of the fiber-fed mode, we get a spectral resolution of 50,000. Typical exposure times of the observations of HD 40956 and HD 111591 at OAO are 25 and 15 minutes with HIDES-slit and HIDES-fiber modes, respectively, achieving S/Ns of about 170.

Reduction of the HIDES data was done using software packages of the IRAF. The standard reductions of bias subtraction, flat-fielding, order extraction, wavelength calibration, and so on, were performed on each frame. Stellar RV measurements were performed with a modeling technique using an I_2 superposed stellar spectrum detailed in Sato et al. (2002) based on a method of Butler et al. (1996). Stellar templates were made by deconvolutions from pure stellar spectra taken without the I_2 cell with instrumental profiles estimated from I_2 superposed flat spectra (Sato et al. 2007). Typical errors of the RV measurements are about $3.5\text{--}6 \text{ m s}^{-1}$. We obtained 36 and 20 spectra for HD 40956 and HD 111591, respectively.

The RVs of each star derived from BOES and HIDES data are listed in Tables 3, 4, and 5.

3. Stellar properties

The stellar properties of HD 40956, HD 111591, and HD 113996 are summarized in Table 1. Visual magnitude (m_v) and parallax (π) were adopted from van Leeuwen (2007) revised from the *HIPPARCOS* catalog (ESA 1997). The atmospheric parameters (effective temperature T_{eff} , Fe abundance [Fe/H], surface gravity $\log g$, and microturbulent velocity v_{micro}) were derived by the TGVIT (Takeda et al. 2005) program, which uses equivalent width (EW) of Fe I and Fe II lines. The projected rotational velocity $v_{\text{rot}} \sin i$ was estimated by Takeda et al. (2008). The spectral type, RV, and luminosity of these stars were obtained from Anderson & Francis (2012). The stellar radius, mass, and age of each star were calculated by the method of da Silva et al. (2006).

HD 40956 is a K0-type star with an effective temperature of $4869 \pm 28 \text{ K}$, a stellar luminosity of $46.17 L_{\odot}$, and a metallicity [Fe/H] of 0.14 ± 0.05 . It seems to be located on the red clump on the H-R diagram.

Table 1. Stellar parameters for the stars in this study.

Parameter	HD 40956	HD 111591	HD 113996	Ref.
Spectral type	K0	K0 III	K5 III	1
m_v (mag)	6.584 ± 0.001	6.594 ± 0.001	4.918 ± 0.001	1
$B-V$ (mag)	1.011 ± 0.006	1.002 ± 0.002	1.482 ± 0.003	1
RV (km s ⁻¹)	-15.80 ± 0.25	5.67 ± 0.17	-15.72 ± 0.01	2
π (mas)	8.44 ± 0.51	9.22 ± 0.47	9.84 ± 0.22	1
T_{eff} (K)	4869 ± 28	4884 ± 30	4181 ± 40	3
[Fe/H]	0.14 ± 0.05	0.07 ± 0.04	0.13 ± 0.08	3
log g (cgs)	3.02 ± 0.09	3.10 ± 0.10	1.86 ± 0.16	3
v_{micro} (km s ⁻¹)	1.20 ± 0.10	1.23 ± 0.11	1.53 ± 0.14	3
Age (Gyr)	1.35 ± 0.18	1.41 ± 0.14	3.24 ± 1.20	3
R_{\odot} (R_{\odot})	8.56 ± 0.33	8.03 ± 0.49	25.11 ± 1.20	3
M_{\odot} (M_{\odot})	2.00 ± 0.08	1.94 ± 0.07	1.49 ± 0.18	3
L_{\odot} (L_{\odot})	46.17	38.07	291.00	2
$v_{\text{rot}} \sin i$ (km s ⁻¹)	2.7 ± 0.5	3.1 ± 0.5	3.3 ± 0.5	3
$P_{\text{rot}} / \sin i$ (days)	158.9	130.5	389.9	3

References.— (1) van Leeuwen (2007); (2) Anderson & Francis (2012); (3) This work.

Table 2. Orbital parameters for the companions.

Parameter	HD 40956 b	HD 111591 b	HD 113996 b
P (days)	578.6 ± 3.3	1056.4 ± 14.3	610.2 ± 3.8
K (m s ⁻¹)	68 ± 2	59 ± 3	120 ± 9
$T_{\text{periastron}}$ (JD)	2455341.88 ± 11.07	2455602.40 ± 30.85	2453309.94 ± 23.67
e	0.24 ± 0.05	0.26 ± 0.10	0.28 ± 0.12
ω (deg)	338.62 ± 7.74	78.72 ± 11.94	92.06 ± 17.25
$m \sin i$ (M_J)	2.7 ± 0.6	4.4 ± 0.4	6.3 ± 1.0
a (AU)	1.4 ± 0.1	2.5 ± 0.1	1.6 ± 0.1
Slope (m s ⁻¹ yr ⁻¹)	-13×10^{-2}	—	—
N_{obs}	54	44	62
rms (m s ⁻¹) (BOAO)	23.6	19.5	39.3
rms (m s ⁻¹) (OAO)	16.1	9.9	—

HD 111591 is a K0 III-type giant star with an effective temperature of 4884 ± 30 K, a stellar luminosity of $38.07 L_{\odot}$, and a metallicity [Fe/H] of 0.07 ± 0.04 .

HD 113996 is a K5 III-type giant and slightly later than the previous two stars. The star has an effective temperature of 4181 ± 40 K, a stellar luminosity of $291 L_{\odot}$, and a metallicity [Fe/H] of 0.13 ± 0.08 ; it appears to be located on the RGB branch on the H-R diagram. The rotation velocity is estimated to be 3.3 ± 0.5 km s⁻¹.

4. Orbital solutions

Assuming that the RV variation is caused by Keplerian orbital motion by unseen companions, we calculated the orbital parameters using the iterated non-linear least-squares method. During the orbital solution, we included the offset between BOES and HIDES RVs as an unknown parameter. If the RV showed linear variation, we also included a linear slope as an unknown parameter. The parameters of orbital solution are summarized in Table 2.

4.1. HD 40956

The RVs of HD 40956 are listed in Table 3 and shown in Figures 1 and 2. A periodic variation is clearly seen in the RV plot. We

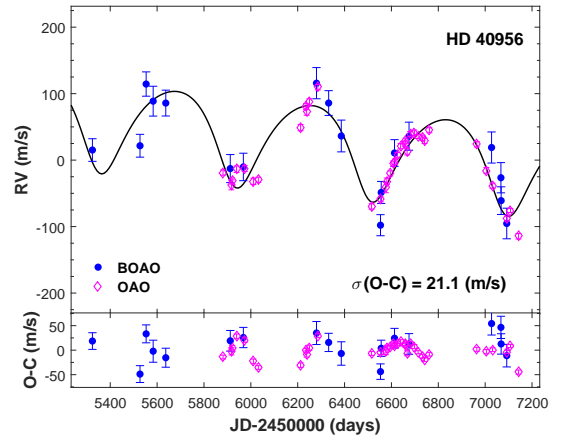


Fig. 1. *Top* : The RVs of HD 40956 observed at BOAO (blue dots) and OAO (magenta diamonds). A Keplerian orbital fit is shown by the solid line. *Bottom* : The residuals after subtracting the orbital motion and a long-term trend from the RVs.

made a Lomb-Scargle (L-S) periodogram to look for a period of the variation (Top panel of Fig. 3) and found a dominant peak around 578 d. The RV also clearly shows a linear trend. Therefore, we included linear slope as an unknown parameter

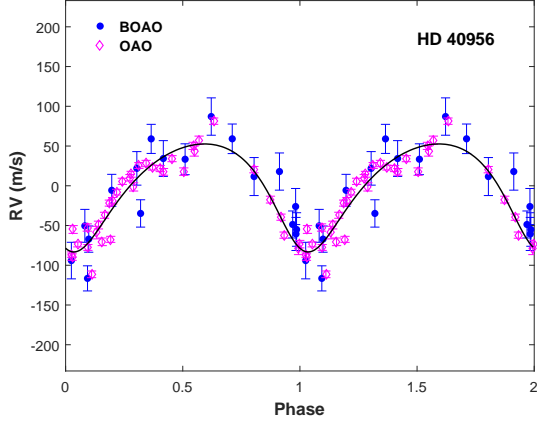


Fig. 2. The phase RV curve folded by an orbital period of 578 d.

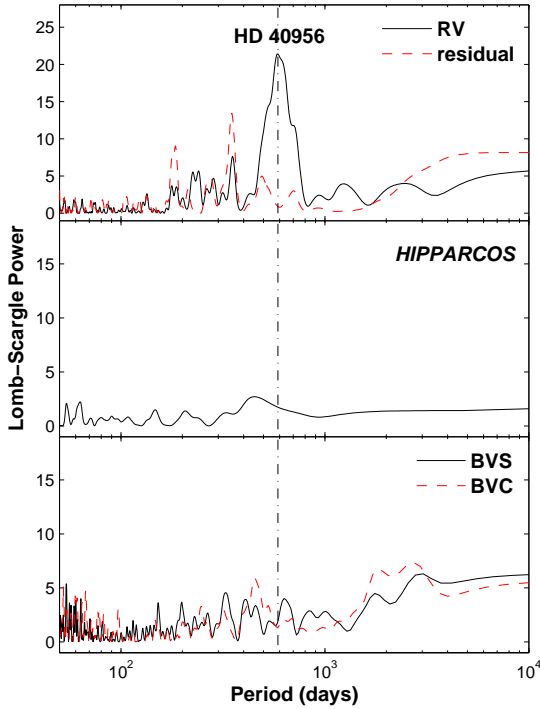


Fig. 3. The L-S periodograms of the RVs and residuals (*top*), *HIPPARCOS* photometries (*middle*), and the line bisector span (BVS, solid line) and curvature (BVC, dash line) (*bottom*) for HD 40956. The vertical dash-dot line indicates an orbital period of 578 d.

during the orbital solution. The orbital fit yields an orbital period of $P = 578.6 \pm 3.0$ d, a semi-amplitude of $K = 68 \pm 2$ m s⁻¹, and an eccentricity of $e = 0.24 \pm 0.05$. Figure 2 shows a phase folded RV of the orbital fit. The rms of the RV residuals after the removal of the orbital motion is 21.1 m s⁻¹, which is somewhat larger than our RV measurement error of 12.4 m s⁻¹. This is not surprising, because most K giant stars show several tens m s⁻¹ of intrinsic RV variation (Sato et al. 2005; Hekker et al. 2006).

There seems to be small periodic variation in the residual as can be seen from the bottom panel of Figure 1. The result of L-S period analysis of the residual shows small peaks at 185 and 352

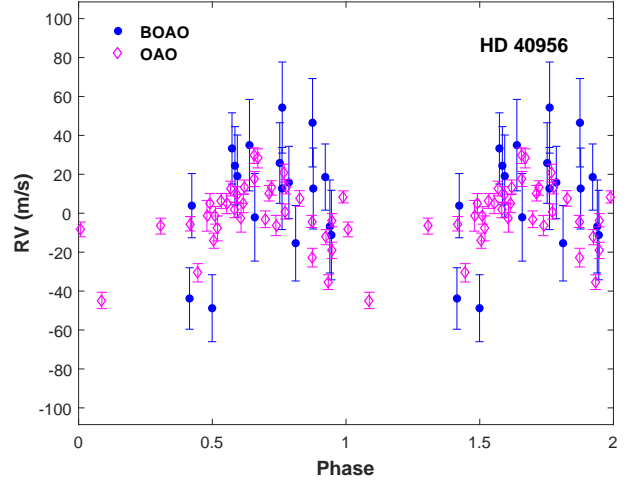


Fig. 4. 360-day period phase folded plot of residual RV of HD 40956.

d (Fig. 3). The 352-day period may be real or alias due to observation bias. As can be seen from Figure 4, most of observations concentrate into one-half of the whole phase for 360-day periodicity. Therefore, we cannot determine the reality of the 352-day period at this stage. Adopting the stellar mass of $2.0 M_{\odot}$, a minimum mass and a semi-major axis of the orbiting companion are estimated: $m \sin i = 2.7 M_J$, $a = 1.4$ AU.

4.2. HD 111591

The RVs of HD 111591 are shown in Figure 5. A periodic variation is clearly seen in the RV measurements. We performed a L-S period analysis and found a significant peak around 1056 d in the periodogram. The orbital fit yields a period of $P = 1056.4 \pm 14.3$ d, a semi-amplitude of $K = 59 \pm 3$ m s⁻¹, and an eccentricity of $e = 0.26 \pm 0.10$. The rms of the RV residuals after the removal of the 1056 d orbital motion is 21.9 m s⁻¹. The residual does not show any significant periodicity (Fig. 7). Adopting the stellar mass of $1.9 M_{\odot}$, a minimum mass and a semi-major axis of the orbiting companion are estimated: $m \sin i = 4.4 M_J$, $a = 2.5$ AU.

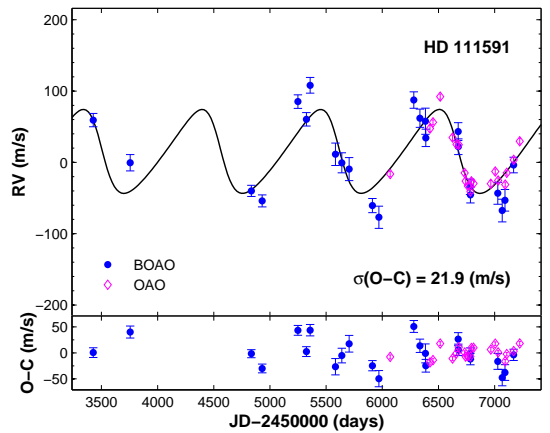


Fig. 5. *Top* : The RVs of HD 111591 observed at BOAO (blue dots) and OAO (magenta diamonds). A Keplerian orbital fit is shown by the solid line. *Bottom* : The RV residuals after the orbital fit.

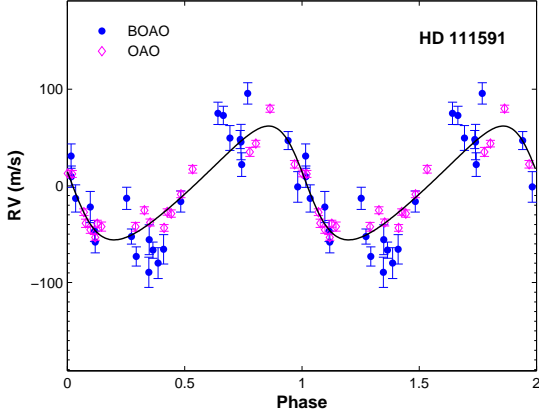


Fig. 6. The phase RV curve folded by an orbital period of 1056 d.

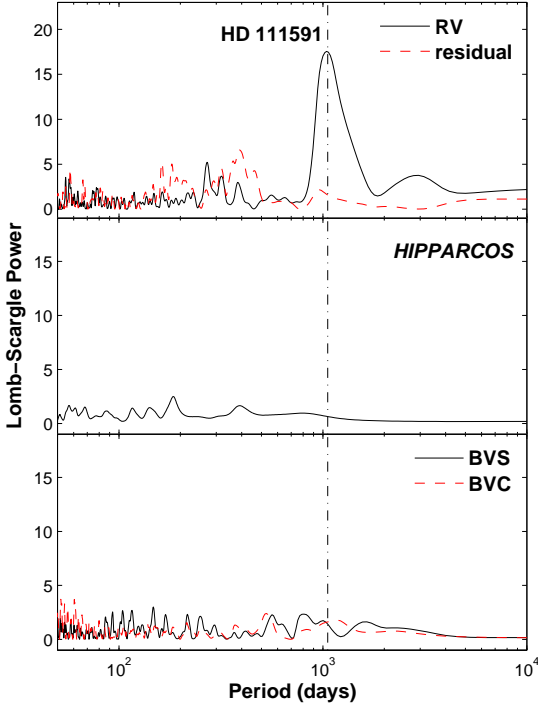


Fig. 7. The L-S periodograms of the RVs and residuals (*top*), *HIPPARCOS* photometries (*middle*), and the line bisector span (BVS, solid line) and curvature (BVC, dash line) (*bottom*) for HD 111591. The vertical dash-dot line indicates an orbital period of 1056 d.

4.3. HD 113996

The RVs of HD 113996 are shown in Figure 8. We performed a L-S period analysis and found a significant peak around 610 d. The orbital fit yields an orbital period of $P = 610.2 \pm 3.8$ d, a semi-amplitude of $K = 120 \pm 9$ m s⁻¹, and an eccentricity of $e = 0.28 \pm 0.12$. The rms residual after the orbital fit is

39.3 m s⁻¹, which is larger than 21 m s⁻¹ of HD 40956 and HD 111591. This is not surprising since HD 113996 is K5 which is later than K0 of HD 40956 and HD 111591. In general, later spectral giant stars show larger intrinsic RV variations. The residual does not show any significant periodicity (Fig. 10). Adopting a stellar mass of $1.49 M_{\odot}$, a minimum mass and a semi-major axis of the orbiting companion are estimated: $m \sin i = 6.3 M_J$, $a = 1.6$ AU.

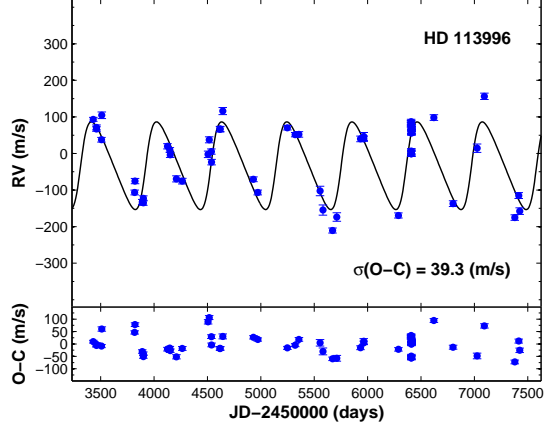


Fig. 8. *Top* : The RVs of HD 113996 observed at BOAO (blue dots). A Keplerian orbital fit is shown by the solid line. *Bottom* : The RV residuals after the orbital fit.

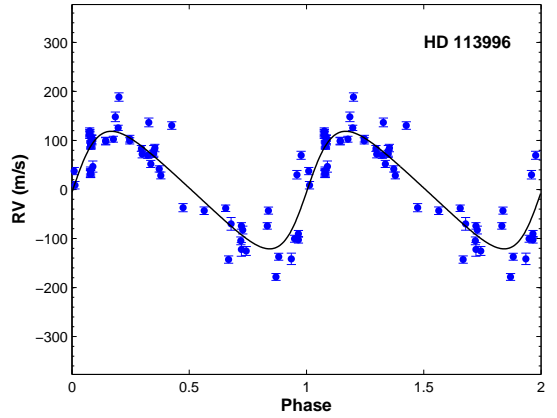


Fig. 9. The phase RV curve folded by an orbital period 610 d.

5. Stellar activity and pulsation diagnostics

The RV variations of the stars may be due to some intrinsic nature of the stars, such as stellar pulsation, chromospheric activity, and rotational modulation of surface features. In this Section, we present the investigation of chromospheric activity, photometric, and line shape variation. We also discuss the possibility of pulsation of the stars.

5.1. Chromospheric activity

To check the stellar activity of the program stars, we show a Ca II H line of each star in Figure 11, which is a sensitive indi-

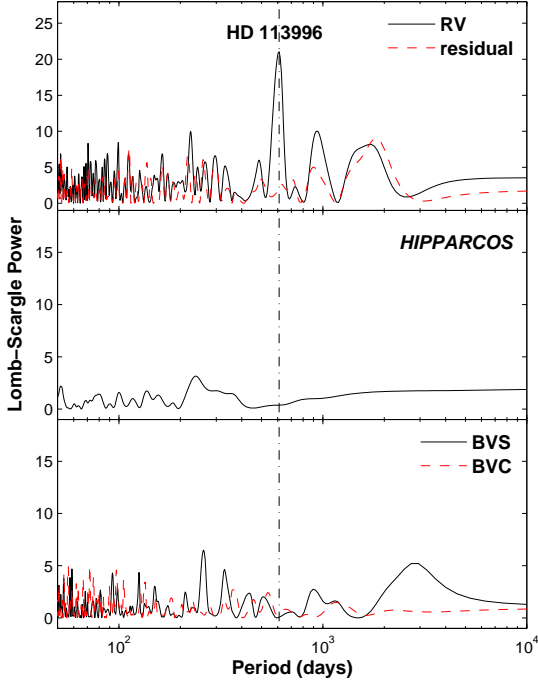


Fig. 10. The L-S periodograms of the RVs and residuals (*top*), *HIPPARCOS* photometries (*middle*), and the line bisector span (BVS, solid line) and curvature (BVC, dash line) (*bottom*) for HD 113996. The vertical dash-dot line indicates a period of 610 d.

cator of chromospheric activity. As seen in Figure 11, we could not find any significant emission in the line core of each star. Although there seems to be a slight reversal in the core of the line of HD 113996, it is negligible compared to the line core of active star HD 201096.

5.2. *HIPPARCOS* photometry

To investigate the photometric variations of the stars, we used *HIPPARCOS* photometric data. From the *HIPPARCOS* catalog, we used 126, 93, and 112 photometric observations for HD 40956, HD 111591, and HD 113996, respectively. The rms scatters are 0.012, 0.011, and 0.005 mag, respectively. The rms scatter seems to be comparable to the uncertainty of photometric data which is about 0.005 to 0.008 mag. We calculated L-S periodogram of the *HIPPARCOS* photometric data, and could not find any periodicity consistent with the RV periods presented in Section 4.

5.3. Line-shape variation

Another technique to investigate the cause of the RV variations is to check the line-shape variations. Line-shape variations, pulsations, rotational modulation, and inhomogeneous surface features due to spots or plagues. In order to investigate the line-shape variations, we calculated two quantities. One is a bisector velocity span ($BVS = V_{top} - V_{bottom}$), which is a velocity difference between flux levels at 0.4 and 0.8 times the continuum level. The other is a velocity curvature ($BVC = [V_{top} - V_{center}] - [V_{center} - V_{bottom}]$), which is the difference between veloc-

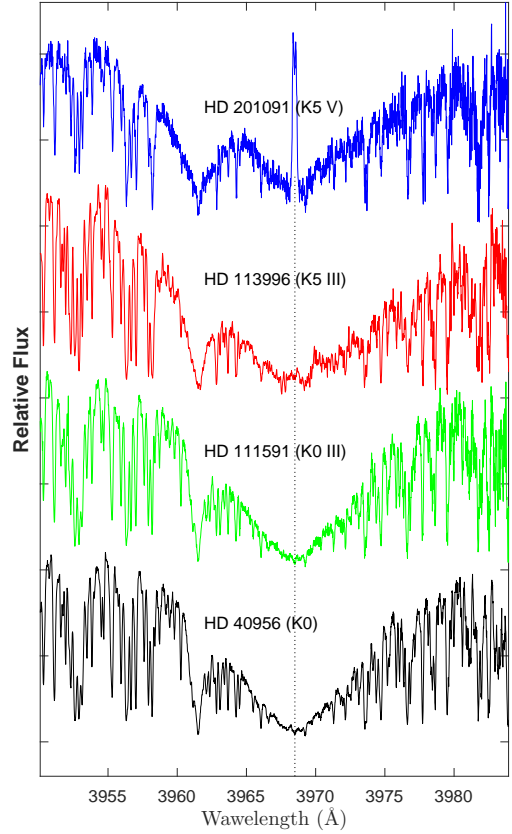


Fig. 11. Spectra of Ca II H lines of the HD 40956, HD 111591, and HD 113996. For comparison, we show the spectra of an active K5-type giant star HD 201096 at the top of Figure. The vertical dotted line indicates the center of the Ca II H line (3968.5 Å).

ity spans in the upper half and the lower half. For the bisector analysis, we selected several lines (Ca I 6122.2, 6439.1, 6462.6, 6717.7; Fe I 6141.7, 6393.6, 6677.9, 6750.2; Fe II 6151.6; Ni I 6643.6, 6767.8; Ti I 6742.6) in the spectral region of 6000 - 7000 Å, which are relatively strong and free from iodine and telluric lines (Hatzes et al. 2005; Lee et al. 2014b, 2015). We performed L-S period analysis for BVS and BVC as shown in the bottom panels of Figures 3, 7, and 10 and could not find any periodicity of line-shape variations consistent with those of the RV variations. To investigate the correlation between RV variations and line bisectors, we plotted the RVs and line bisector values in Figure 12. Although the uncertainties of the line bisector values are large, we cannot see any clear correlation between RV and line bisector.

5.4. Pulsations

There are some K giants that are known to be pulsating stars, which have several oscillation modes at different frequencies with different amplitudes. The pulsation periods can range from hours to days depending on the radius and mass of the star. For radial pulsations, we can use the Q-constant formulae of Xiong & Deng (2007) to calculate the period, which results in $P_{osc} \sim 0.58$ d for HD 40956, $P_{osc} \sim 0.31$ d for HD 111591, and $P_{osc} \sim 4.78$ d for HD 113996.

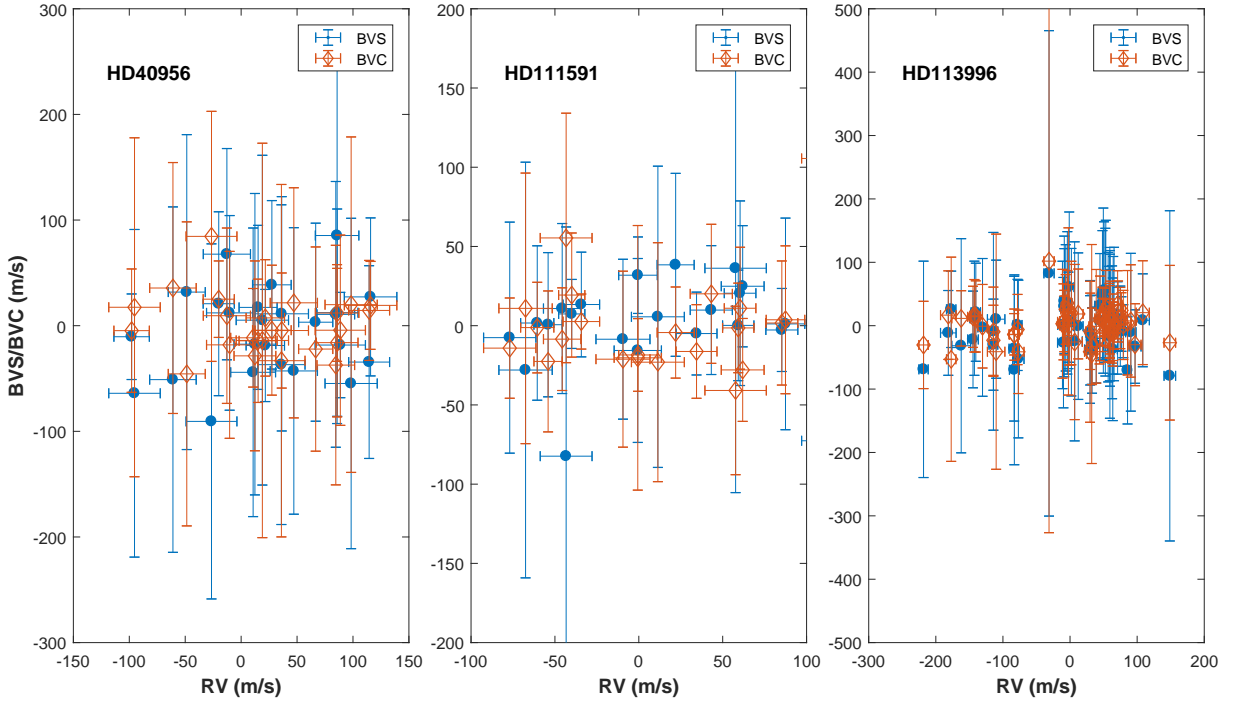


Fig. 12. Line bisector measurements versus RV.

The periods for p-mode non-radial pulsations can be estimated from the scaling relationships for ν_{max} , the frequency of maximum pulsation power, which is given by $\nu_{max} \sim 3.05 (M/R^2)$ mHz. The estimation yields $P_{osc} \sim 3.3$ h for HD 40956, $P_{osc} \sim 3$ h for HD 111591, and $P_{osc} \sim 1.6$ d for HD 113996.

All these periods are much less than the long RV periods found in this study, so we can exclude traditional oscillations as the cause of the RV variations. However some authors report pulsation periods for K and M giant stars of several hundred days; for example, Lee et al. (2016) found a 473 d periodic RV variation for M-giant binary μ UMa. They found a correlation between the RV variations and the equivalent widths of $H\alpha$ and $H\beta$ lines, and thus concluded that the detected RV variations of μ UMa are caused by non-radial pulsation. Saio et al. (2015) also found possible convective oscillation modes in three low-mass luminous red giants in LMC and the modes can be explained by sequence D pulsations. Hatzes et al. (2017, priv. comm.) found long-period variations in γ Dra possibly caused by pulsations. The mechanism of these long-period pulsation of giant stars is not well understood yet. We therefore reserve the possibility of pulsations as the cause of long-period RV variation of giant stars.

6. Summary and Discussion

We clearly detected long-period RV variations in three K giant stars. In order to confirm the nature of these periodic RV variations, we checked *HIPPARCOS* photometric data, chromospheric activity, line-shape variations, and rotational period. These analyses do not show any clear correlation with the RV variations and the rotational periods are much shorter than the observed RV variation periods. Though we don't exclude pulsation as the cause of the RV variations, as discussed in the previous Section, we conclude that the periodic RV variations are most likely caused by substellar companions. We performed orbital analysis and found the period and companion mass; $P = 578.6 \pm 3.3$ d, $m \sin i = 2.7 \pm 0.6 M_J$ for HD 40956; $P = 1056.4$

± 14.3 d, $m \sin i = 4.4 \pm 0.4 M_J$ for HD 111591; $P = 610.2 \pm 3.8$ d, $m \sin i = 6.3 \pm 1.0 M_J$ for HD 113996.

HD 40956 shows complex RV variations with a period of 578.6 d and a long-term linear RV trend of $13 \text{ m s}^{-1} \text{ yr}^{-1}$, which may be related to a long-period companion. The residuals, after subtracting a 578-day orbital motion, show weak 185-day periodicity. At this moment, the reality and cause of this periodicity are not clear. We need more follow-up observations to clarify these issues. We note that among the planetary systems around giant stars, some systems with two giant planets are found with orbital periods similar to a period ratio of 360 d and 580 d and stable orbits (Johnson et al. 2011, Trifonov et al. 2014, Sato et al. 2016). HD 40956 of this study may add one more example similar to these planetary systems with a period of 185 d instead of 360 d.

HD 111591 has a period of 1056.4 d, which is the longest among the three stars in this study. Although this long period is comparable to the luminous Mira-type variables, taking into account the spectral type and surface gravity of this star, we exclude the Mira-type pulsations as the explanation of the RV variations. No additional significant periodicity was found in the residual RV after the orbital fit.

The rms residual after the orbital fit of HD 113996 is 39.3 m s^{-1} , which is about twice larger than that for the other K0 giants in this study. As mentioned earlier, it is not surprising that later spectral-type giant stars in general show larger intrinsic RV variations (HD 113996 is K5 III star). In fact, the typical intrinsic RV variation of K5 stars is larger than 50 m s^{-1} ; the K5 III star α Tau, for example, shows about 80 m s^{-1} intrinsic RV variations (Hatzes et al. 2015).

Acknowledgements. This work is supported by the KASI (Korea Astronomy and Space Science Institute) through grant No. 2016-1-860-02. This work was in part supported by JSPS (Japan Society for the Promotion of Science) KAKENHI Grant Numbers 23244038, 16H02169. BCL acknowledges partial support by the KASI grant 2016-1-832-01. This research made use of the SIMBAD database, operated at the CDS, Strasbourg, France. Data analysis was in part carried out on the open use data analysis computer system at the Astronomy Data Center,

ADC, of the National Astronomical Observatory of Japan. We thank all officials of BOAO and OAO. We also thank an anonymous referee for helpful comments and suggestions to greatly improve the paper.

References

- Anderson, E., & Francis, C. 2012, *Astronomy Letters*, 38, 331
- Butler, R. P., Marcy, G. W., Williams, E., McCarthy, C., Dosanji, P., & Vogt, S. S. 1996, *PASP*, 108, 500
- Collier Cameron, A., et al. 2010, *MNRAS*, 407, 507
- da Silva, L., et al. 2006, *A&A*, 458, 609
- ESA. 1997, *VizieR Online Data Catalog*, 1239
- Ford, E. B., et al. 2011, *ApJS*, 197, 2
- Frink, S., Mitchell, D. S., Quirrenbach, A., Fischer, D. A., Marcy, G. W., & Butler, R. P. 2002, *ApJ*, 576, 478
- Gaudi, B. S., et al. 2017, *Nature*, 546, 514
- Han, I., Kim, K.-M., Byeong-Cheol, L., & Valyavin, G. 2007, *Publication of Korean Astronomical Society*, 22
- Han, I., Lee, B.-C., Kim, K.-M., & Mkrtichian, D. E. 2008, *Journal of Korean Astronomical Society*, 41, 59
- Han, I., Lee, B. C., Kim, K. M., Mkrtichian, D. E., Hatzes, A. P., & Valyavin, G. 2010, *A&A*, 509, A24
- Hartman, J. D., et al. 2015, *AJ*, 150, 197
- Hatzes, A. P., & Cochran, W. D. 1993, *ApJ*, 413, 339
- Hatzes, A. P., et al. 2015, *A&A*, 580, A31
- Hatzes, A. P., Guenther, E. W., Endl, M., Cochran, W. D., Döllinger, M. P., & Bedalov, A. 2005, *A&A*, 437, 743
- Hekker, S., Reffert, S., Quirrenbach, A., Mitchell, D. S., Fischer, D. A., Marcy, G. W., & Butler, R. P. 2006, *A&A*, 454, 943
- Izumiura, H. 1999, *Publications of the Yunnan Observatory*, 77
- Izumiura, H. 2005, *Journal of Korean Astronomical Society*, 38, 81
- Johnson, J. A., et al. 2011, *AJ*, 141, 16
- Kambe, E., et al. 2002, *PASJ*, 54, 865
- Kambe, E., et al. 2013, *PASJ*, 65, 15
- Kim, K.-M., et al. 2007, *PASP*, 119, 1052
- Lee, B.-C., Han, I., & Park, M.-G. 2013, *A&A*, 549, A2
- Lee, B.-C., Han, I., Park, M.-G., Mkrtichian, D. E., Hatzes, A. P., Jeong, G., & Kim, K.-M. 2016, *AJ*, 151, 106
- Lee, B.-C., Han, I., Park, M.-G., Mkrtichian, D. E., Hatzes, A. P., & Kim, K.-M. 2014a, *A&A*, 566, A67
- Lee, B.-C., Han, I., Park, M.-G., Mkrtichian, D. E., Jeong, G., Kim, K.-M., & Valyavin, G. 2014b, *Journal of Korean Astronomical Society*, 47, 69
- Lee, B.-C., et al. 2015, *A&A*, 584, A79
- Omiya, M., et al. 2012, *PASJ*, 64, 34
- Omiya, M., et al. 2009, *PASJ*, 61, 825
- Reffert, S., Bergmann, C., Quirrenbach, A., Trifonov, T., & Künstler, A. 2015, *A&A*, 574, A116
- Saio, H., Wood, P. R., Takayama, M., & Ita, Y. 2015, *MNRAS*, 452, 3863
- Sato, B., et al. 2007, *ApJ*, 661, 527
- Sato, B., Kambe, E., Takeda, Y., Izumiura, H., & Ando, H. 2002, *PASJ*, 54, 873
- Sato, B., Kambe, E., Takeda, Y., Izumiura, H., Masuda, S., & Ando, H. 2005, *PASJ*, 57, 97
- Sato, B., et al. 2012, *PASJ*, 64, 135
- Sato, B., et al. 2016, *ApJ*, 819, 59
- Takeda, Y., Ohkubo, M., Sato, B., Kambe, E., & Sadakane, K. 2005, *PASJ*, 57, 27
- Takeda, Y., Sato, B., & Murata, D. 2008, *PASJ*, 60, 781
- Trifonov, T., Reffert, S., Tan, X., Lee, M. H., & Quirrenbach, A. 2014, *A&A*, 568, A64
- van Leeuwen, F. 2007, *A&A*, 474, 653
- Xiong, D. R., & Deng, L. 2007, *MNRAS*, 378, 1270
- Zhou, G., et al. 2017, *AJ*, 153, 211
- Zhou, G., et al. 2016, *AJ*, 152, 136

Table 3. RV measurements for HD 40956

JD -2450000	ΔRV $m s^{-1}$	$\pm\sigma$ $m s^{-1}$	Observatory / Spectrograph
5323.9789	15.2	17.0	BOAO / BOES
5527.0623	21.6	17.2	BOAO / BOES
5553.2149	114.4	18.3	BOAO / BOES
5583.1940	88.7	22.5	BOAO / BOES
5636.9949	85.8	19.4	BOAO / BOES
5881.3676	-18.7	3.9	OAO / HIDES slit
5912.2101	-12.7	21.1	BOAO / BOES
5917.1522	-37.2	7.4	OAO / HIDES slit
5920.1383	-31.4	4.7	OAO / HIDES slit
5939.1603	-13.8	4.9	OAO / HIDES slit
5968.0579	-10.3	20.7	BOAO / BOES
5974.0024	-12.6	4.6	OAO / HIDES slit
6010.9628	-31.9	4.8	OAO / HIDES slit
6031.9598	-29.6	3.8	OAO / HIDES slit
6212.3446	48.9	4.7	OAO / HIDES slit
6235.3600	80.5	4.5	OAO / HIDES slit
6238.2177	73.9	6.4	OAO / HIDES slit
6250.1645	87.0	5.2	OAO / HIDES slit
6280.1870	115.7	23.5	BOAO / BOES
6286.1746	109.8	4.0	OAO / HIDES slit
6332.0850	85.9	18.6	BOAO / BOES
6385.9881	36.3	23.9	BOAO / BOES
6515.3211	-69.7	4.1	OAO / HIDES fiber
6553.3025	-97.9	15.8	BOAO / BOES
6554.2186	-59.0	3.7	OAO / HIDES fiber
6556.3094	-48.6	16.5	BOAO / BOES
6576.2283	-41.2	7.9	OAO / HIDES slit
6580.2782	-31.8	4.9	OAO / HIDES slit
6595.2285	-20.1	3.8	OAO / HIDES fiber
6607.1773	-5.2	3.8	OAO / HIDES fiber
6613.0858	10.7	20.1	BOAO / BOES
6615.3592	-2.6	4.1	OAO/HIDES fiber
6625.1445	7.9	3.6	OAO / HIDES fiber
6639.1269	21.0	3.9	OAO / HIDES fiber
6658.0666	24.8	4.0	OAO / HIDES fiber
6661.0665	29.1	3.7	OAO / HIDES fiber
6667.0308	13.0	5.2	OAO / HIDES slit
6675.0717	36.0	21.1	BOAO / BOES
6680.0901	39.4	3.7	OAO / HIDES fiber
6697.9855	41.2	4.0	OAO / HIDES fiber
6713.9426	35.6	3.0	OAO / HIDES fiber
6732.9673	33.6	3.9	OAO / HIDES fiber
6740.9561	29.2	4.2	OAO / HIDES slit
6761.9766	45.0	3.8	OAO / HIDES fiber
6964.2531	23.8	4.0	OAO / HIDES fiber
7005.1077	-15.5	4.3	OAO / HIDES fiber
7027.3119	19.0	23.4	BOAO / BOES
7031.1283	-38.5	3.9	OAO / HIDES slit
7067.2337	-26.5	22.7	BOAO / BOES
7068.1621	-61.0	20.8	BOAO / BOES
7092.0618	-95.3	23.0	BOAO / BOES
7092.9540	-87.9	3.4	OAO / HIDES fiber
7108.0408	-75.7	3.1	OAO / HIDES fiber
7141.9433	-114.5	4.2	OAO / HIDES fiber

Table 4. RV measurements for HD 111591

JD -2450000	ΔRV $m s^{-1}$	$\pm\sigma$ $m s^{-1}$	Observatory/Spectrograph
3427.3029	59.3	9.3	BOAO / BOES
3756.3732	-0.5	11.5	BOAO / BOES
4834.3355	-40.0	7.8	BOAO / BOES
4931.0714	-54.1	8.4	BOAO / BOES
5248.3155	85.3	9.5	BOAO / BOES
5324.1067	60.4	9.4	BOAO / BOES
5358.0604	108.1	11.0	BOAO / BOES
5583.3769	11.4	15.8	BOAO / BOES
5639.1594	-0.6	14.1	BOAO / BOES
5705.0934	-9.4	16.1	BOAO / BOES
5912.3642	-60.5	9.9	BOAO / BOES
5969.3377	-76.9	15.6	BOAO / BOES
6070.1044	-16.3	3.8	OAO / HIDES slit
6280.3748	87.4	11.5	BOAO / BOES
6334.3126	61.9	12.8	BOAO / BOES
6384.1195	57.7	18.3	BOAO / BOES
6387.0977	34.4	12.2	BOAO / BOES
6424.1126	47.5	4.7	OAO / HIDES slit
6451.0005	56.2	3.4	OAO / HIDES slit
6514.9560	92.2	3.7	OAO / HIDES fiber
6625.3257	34.8	3.9	OAO / HIDES fiber
6660.3878	25.2	3.4	OAO / HIDES fiber
6675.3470	43.2	12.6	BOAO / BOES
6676.3999	22.0	11.0	BOAO / BOES
6680.2737	24.8	3.6	OAO / HIDES fiber
6733.0800	-14.8	3.5	OAO / HIDES fiber
6741.1461	-26.3	4.3	OAO / HIDES slit
6762.1124	-33.1	3.6	OAO / HIDES fiber
6781.1942	-34.3	10.9	BOAO / BOES
6784.1022	-40.9	3.0	OAO / HIDES fiber
6784.1229	-45.7	11.2	BOAO / BOES
6793.1269	-26.6	3.6	OAO / HIDES fiber
6812.1034	-29.7	4.7	OAO / HIDES fiber
6965.3508	-29.9	4.5	OAO / HIDES fiber
7005.2581	-12.9	3.6	OAO / HIDES fiber
7027.2939	-43.3	15.4	BOAO / BOES
7031.2874	-25.5	3.6	OAO / HIDES slit
7067.2528	-67.5	15.9	BOAO / BOES
7092.0811	-53.2	15.2	BOAO / BOES
7094.1016	-31.1	3.5	OAO / HIDES fiber
7108.1564	-14.6	3.3	OAO / HIDES fiber
7169.0409	-3.8	10.9	BOAO / BOES
7170.0352	3.6	3.4	OAO / HIDES fiber
7222.9709	29.6	4.0	OAO / HIDES fiber

Table 5. RV measurements for HD 113996

JD -2450000	ΔRV $m s^{-1}$	$\pm\sigma$ $m s^{-1}$	Observatory / Spectrograph
3430.1733	93.3	5.4	BOAO / BOES
3460.2060	67.0	6.3	BOAO / BOES
3460.2561	71.3	6.8	BOAO / BOES
3507.1163	37.6	6.3	BOAO / BOES
3509.9766	104.5	8.9	BOAO / BOES
3818.1061	-106.6	6.5	BOAO / BOES
3821.0853	-75.4	7.3	BOAO / BOES
3889.1274	-132.8	7.0	BOAO / BOES
3899.0409	-134.9	6.8	BOAO / BOES
3899.1054	-122.8	6.9	BOAO / BOES
4125.2073	19.8	7.2	BOAO / BOES
4147.2649	9.6	6.4	BOAO / BOES
4151.3333	-3.7	7.0	BOAO / BOES
4209.1005	-69.4	8.4	BOAO / BOES
4264.1103	-75.6	7.7	BOAO / BOES
4505.3163	-2.2	8.8	BOAO / BOES
4516.2931	37.4	8.2	BOAO / BOES
4536.1626	5.2	7.3	BOAO / BOES
4538.1339	-23.7	7.6	BOAO / BOES
4618.0332	67.2	7.1	BOAO / BOES
4618.0405	66.0	7.3	BOAO / BOES
4643.1020	116.0	9.8	BOAO / BOES
4930.0810	-70.6	6.6	BOAO / BOES
4971.0880	-106.6	6.5	BOAO / BOES
5248.1945	70.3	6.0	BOAO / BOES
5321.0988	51.5	6.0	BOAO / BOES
5356.1121	52.2	7.6	BOAO / BOES
5554.3842	-102.5	13.0	BOAO / BOES
5581.1788	-154.6	14.0	BOAO / BOES
5671.2112	-210.7	6.9	BOAO / BOES
5711.1867	-173.8	11.6	BOAO / BOES
5933.3180	39.9	7.8	BOAO / BOES
5963.2053	40.4	7.2	BOAO / BOES
5963.3409	46.6	10.9	BOAO / BOES
6288.3860	-169.5	7.0	BOAO / BOES
6407.0292	82.5	6.3	BOAO / BOES
6407.0368	87.0	6.4	BOAO / BOES
6407.0442	84.2	5.9	BOAO / BOES
6407.0517	79.2	6.2	BOAO / BOES
6407.0591	78.5	6.7	BOAO / BOES
6409.0348	-0.8	7.2	BOAO / BOES
6409.0422	6.4	7.1	BOAO / BOES
6409.0497	3.6	6.6	BOAO / BOES
6409.0571	-1.0	7.0	BOAO / BOES
6409.0646	1.2	7.4	BOAO / BOES
6410.0079	58.3	6.3	BOAO / BOES
6410.0154	57.2	5.5	BOAO / BOES
6410.0228	60.2	5.9	BOAO / BOES
6410.0302	60.9	6.2	BOAO / BOES
6410.0376	55.9	6.4	BOAO / BOES
6412.1810	73.2	6.0	BOAO / BOES
6412.1954	71.9	5.9	BOAO / BOES
6412.2098	66.9	6.6	BOAO / BOES
6412.2242	64.4	5.9	BOAO / BOES
6412.2386	67.1	6.1	BOAO / BOES
6620.3166	98.2	7.7	BOAO / BOES
6800.1058	-137.0	7.9	BOAO / BOES
7025.2713	14.5	11.4	BOAO / BOES
7093.0806	156.3	8.6	BOAO / BOES
7378.3318	-175.2	7.4	BOAO / BOES
7415.1456	-115.0	8.0	BOAO / BOES
7424.2282	-157.7	9.0	BOAO / BOES